ELECTRONIC SUPPLEMENTARY INFORMATION

Unexpected persistence of cis-bridged chains in compressed AuF_3

Dominik Kurzydłowski,[*a,b] Serhiy Kobyakov,[a] Zoran Mazej,[c] Sharad Babu Pillai, [d] Brahmananda Chakraborty, [e] Prafulla K. Jha [d]

[a.] *Faculty of Mathematics and Natural Sciences, Cardinal Stefan Wyszyński University, Warsaw 01-038 , Poland*

[b.] *Centre of New Technologies, University of Warsaw, ul. Banacha 2c, Warsaw 02-097, Poland*

[c.] *Department of Inorganic Chemistry and Technology, Jožef Stefan Institute, SI-1000 Ljubljana, Slovenia*

[d.] *Department of Physics, Faculty of Science, The Maharaja Sayajirao University of Baroda, Vadodara 390002, India*

[e.] *High Pressure and Synchrotron Radiation Physics Division, Bhabha Atomic Research Centre, Trombay, Mumbai 400085, India*

Experimental and computational details 2

Tables 5

Figures 6

Crystal structure of the novel high-pressure polymorphs of AuF_3 10

References 12

Experimental and computational details

Raman spectroscopy: Raman spectra were acquired at room temperature with the Alpha300M+ confocal microscope (Witec Gmbh) equipped with a motorized stage. We used a 532 nm laser line delivered to the microscope through a single-mode optical fiber. In order to avoid laser-induced decomposition of AuF_3 the laser power at the sample did not exceed 2 mW. The Raman signal was collected through a 20× long working distance objective, and passed through a multi-mode optical fiber (50 μm core diameter) to a lens-based spectrometer (Witec UHTS 300, f/4 aperture, focal length 300 mm) coupled with a back-illuminated Andor iDUS 401 detector thermoelectrically cooled to -60°C. The spectra were collected with the use of a 1800 mm grating resulting in a 1.2 cm^{-1} spectral resolution. Typical acquisition times ranged from 1 to 5 s with 20 to 30 accumulations. The spectra were post-processed (background subtraction and cosmic-ray removal) with the Project FIVE software (Witec Gmbh). For each pressure point in each experimental run (see Fig. S 5) the position of Raman bands was established with the Fityk 1.3.1 software by fitting the observed bands with Pseudo-Voigt profiles.[1]

High-pressure experiments: A total of six high-pressure runs were conducted with the use of a diamond anvil cell (DAC) equipped with low-fluorescence Ia diamonds with a 500 μm culet (bevelled from 600 μm) and a stainless-steel gasket pre-indented to a thickness of 35 μm. The gasket hole with a radius of 120 μm was laser-drilled. Loading of the DAC with powdered AuF_3 and sealing was performed in an Ar-atmosphere glovebox. The pressure inside the cell was determined from the shift of the R1 ruby fluorescence line.[2] In those cases when the signal from ruby could not be acquired the pressure was determined from the shift of the first-order Raman peak of the diamond anvil tip.[3] AuF_3 decomposition or possible reaction with the diamonds, ruby, and gasket were ruled out by performing Raman mapping (2D scans) of the entire sample at selected pressures.

Synthesis of AuF_3: Gold(III) fluoride was prepared by fluorination of $AuCl_3$ with elemental fluorine in anhydrous hydrogen fluoride. In a typical reaction, 2 g of $AuCl_3$ was weighed into reaction vessel (V = 35 ml) inside a dry-box. Anhydrous HF (7 ml) was condensed onto the reaction mixture at 77 K and the reaction vessel was warmed to ambient temperature. Elemental fluorine was slowly added to the reaction vessel until the pressure of 4 bar was attained. The reaction mixture was allowed to stir at ambient temperature. After one day, the volatiles were partially pumped away until the pressure in the reaction vessel was equal to that of vapour pressure of liquid HF at ambient temperature. After the reaction mixture was warmed to ambient temperature again, the new portion of fluorine was added

again. The whole procedure has been repeated two more times. With the last portion of fluorine, which was already in an excess, the reaction mixture was left for four days.

DFT calculations: Periodic DFT calculations of the geometry and enthalpy of various polymorphs of AuF_3 up to 100 GPa utilized the SCAN meta-GGA functional.[4] We found it to reproduce very well the geometry and vibrational frequencies of the ambient-pressure structure ($P6_122$ symmetry)[5] of AuF_3 (see Table S1). The projector-augmented-wave (PAW) method was used in the calculations,[6] as implemented in the VASP 5.4 code.[7,8] The cut-off energy of the plane waves was set to 800 eV with a self-consistent-field convergence criterion of 10^{-6} eV. Valence electrons (Au: $5d^{10}$, $6s^1$; F: $2s^2$, $2p^5$) were treated explicitly, while standard VASP pseudopotentials, accounting for scalar relativistic effects were used for the description of core electrons. The *k*-point mesh spacing was set to $2\pi \times 0.04$ $Å^{-1}$. All structures were optimized until the forces acting on the atoms were smaller than 5 meV/Å.

Evolutionary algorithm searches were performed in order to identify candidates for high-pressure phases of AuF_3. For this we used the XtalOpt software (version r12)[9] coupled with periodic DFT calculations utilizing the PBE functional.[10] These searches were conducted at 10/40/80 GPa for $Z = 2$, 4, and 6. Thermodynamic stability of various AuF_3 polymorphs was judged by comparing their enthalpy (H), and thus the calculations formally correspond to $T = 0$K at which the Gibbs free energy ($G = H - S \cdot T$, where S is the entropy) is equal to H.

Calculations of Γ-point vibration frequencies were conducted in VASP 5.4 utilizing the SCAN functional. The finite-displacement method was used with a 0.007 Å displacement, and a tighter SCF convergence criterion (10^{-8} eV). In case of the $P6_1$ and $P6_122$ structures we additionally calculated the intensity of Raman-active modes using density-functional perturbation theory (DFPT),[11] as implemented in the CASTEP code (academic release version 19.11).[12] In these calculations the LDA approximation was used together with norm-conserving pseudopotentials (cut-off energy 940 eV). The calculations yielded the Raman activity of each vibrational mode (S_i) from which the relative intensity could be estimated assuming that the intensity of the Raman band is proportional to the following factor[13]:

$$\frac{(\nu_0 - \nu_i)^4}{\nu_i\left(1 - e^{-h\nu_i c/kT}\right)} S_i$$

where ν_0 is the laser frequency, ν_i is the mode frequency, T is the temperature.

For calculations of the electronic band gap (E_g) of the most stable structure of AuF_3 we employed the Heyd-Scuseria-Ernzerhof (HSE06) functional,[14] which is a hybrid functional mixing the GGA functional of Perdew et al.,[10] with 25% of the Hartree-Fock exchange energy. Calculations were performed for the SCAN-relaxed structures.

Visualization of all structures was performed with the VESTA software package.[15] For symmetry recognition we used the FINDSYM program.[16] Input geometries for CATEP calculations were generated with CIF2Cell.[17] Group theory analysis of the vibrational modes was performed with the use of the Bilbao Crystallographic Server.[18]

Tables

Table S 1 Comparison of the experimental geometry and frequencies of the Raman-active vibrational modes of the ambient pressure structure of AuF_3 (space group *P6₁22*) with data obtained from calculations utilizing the SCAN functional. Cell vectors and Au-F distances are in Å, volume in Å^3, frequencies in cm^{-1}.

Crystal structure			**Raman-active vibrations**			
	Exp. (ref. [5])	**SCAN (this work)**	**SCAN (this work)**		**Exp. (this work)**	**Exp (ref. [19])**
a	5.1508	5.0410 (–2.1 %)	E_2	32		
c	16.2637	16.4871 (+1.4 %)	A_1	34		
V	373.68	362.84 (–2.9 %)	E_1	43		
Au-F_t	1.876	1.893 (+0.9 %)	E_2	59		
Au-F_b	2.000	2.004 (+0.2 %)	E_1	67	65	66
			E_2	93		
			E_1	103	105	
			E_2	131		
			E_1	164	165	164
			E_2	164		
			A_1	181	183	182
			E_1	183		
			E_2	212	213	
			E_1	231		
			E_2	233		
			A_1	237		
			E_2	241		
			E_1	247	254	254
			E_2	430	440	436
			E_1	446		
			A_1	453	451	
			E_1	520	531	
			E_2	520	541	540
			E_1	619	623	622
			E_2	621		
			A_1	624	631	631
			E_2	636	645	644
			E_1	647	657	655

Figures

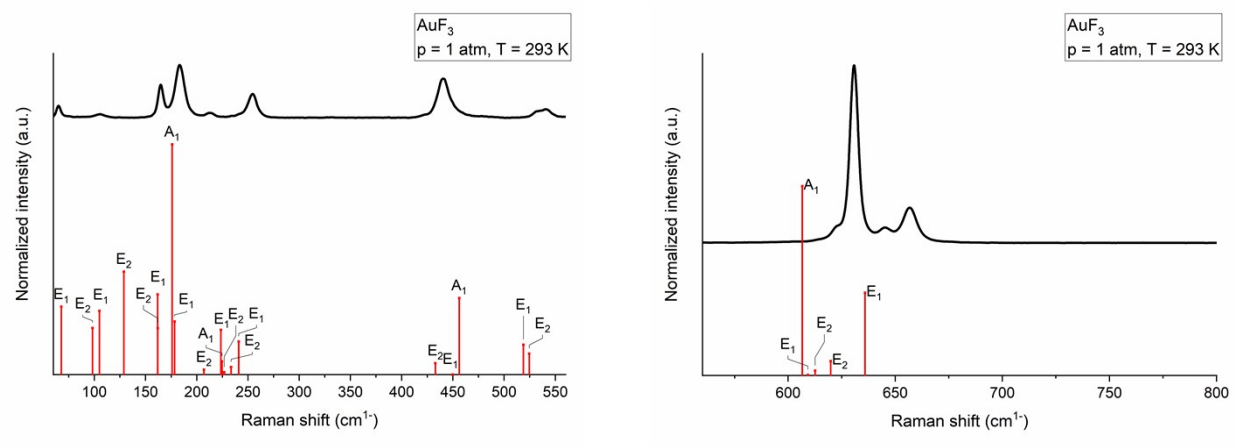

Fig. S 1 Comparison of the experimental Raman spectrum of AuF_3 at 1 atm (black lines) with Raman intensities simulated for the *P6₁22* structure with LDA (red bars). Labels denote symmetry of each mode.

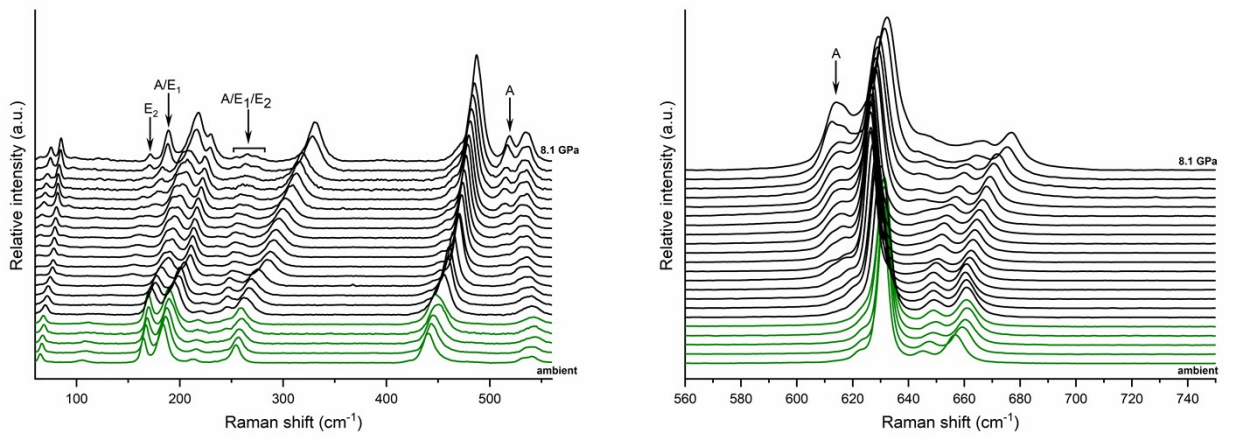

Fig. S 2 Evolution of the Raman spectrum of powdered AuF_3 from ambient pressure to 8.1 GPa (spectra are offset for clarity). Green lines denote spectra corresponding to the *P6₁22* structure, black to the *P6₁* polymorph. The bands originating from the latter structure which are gaining in intensity upon compression are marked with their symmetry.

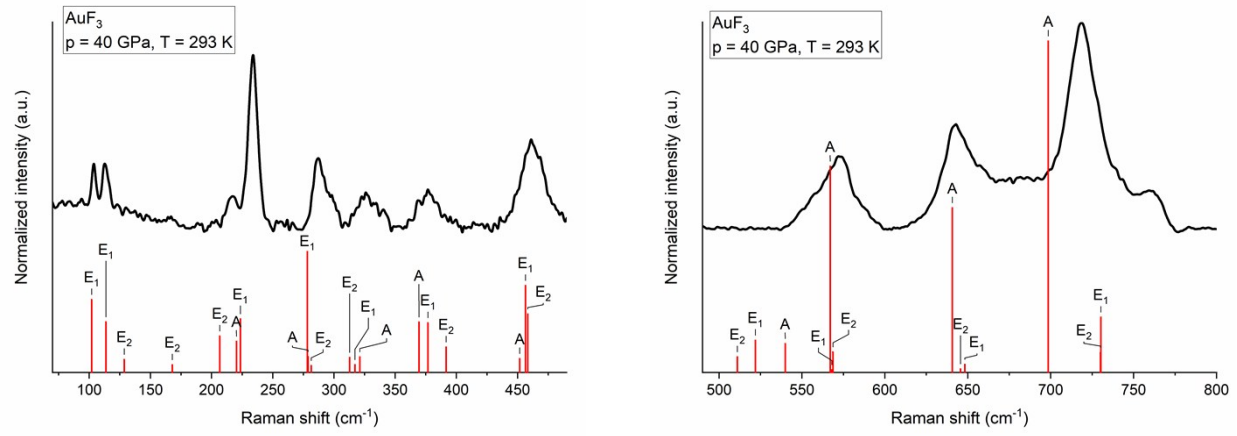

Fig. S 3 Comparison of the experimental Raman spectrum of AuF_3 at 40 GPa (black lines) with Raman intensities simulated for the *P6₁* structure with LDA (red bars). Labels denote the symmetry of each mode.

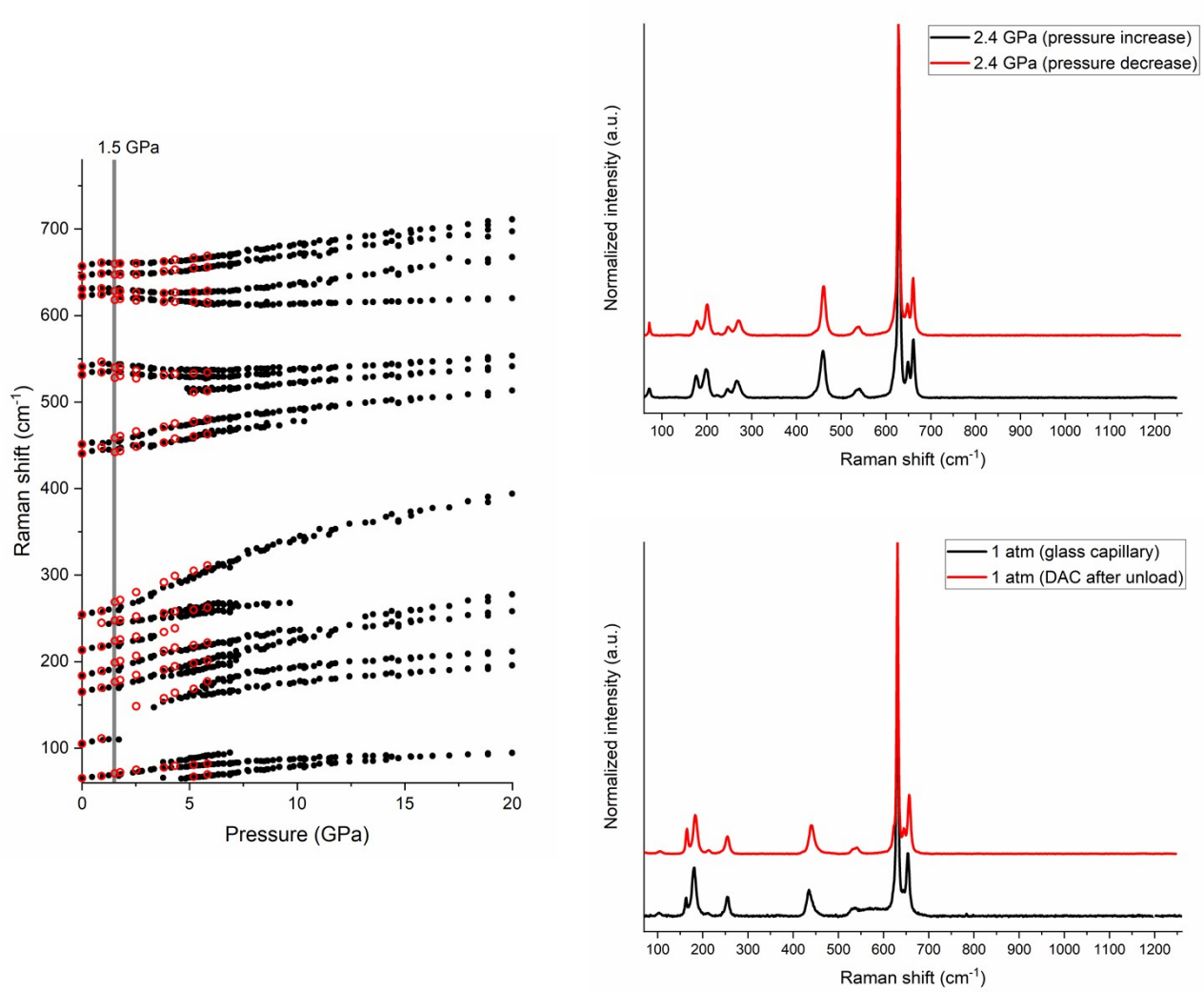

Fig. S 4 Left: comparison of the position of the Raman bands of AuF_3 upon pressure increase (black points) and pressure decrease (red circles). Right: comparison of the Raman spectra upon compression and decompression (upper part) and before and after the high-pressure experiment (lower part). Spectra are offset for clarity

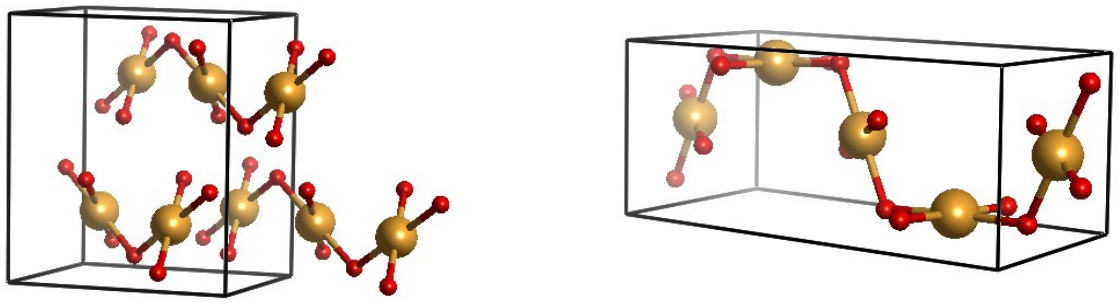

Fig. S 5 The *C2/c(α)* (left) and *C2/c(β)* (right) structures of AuF_3.

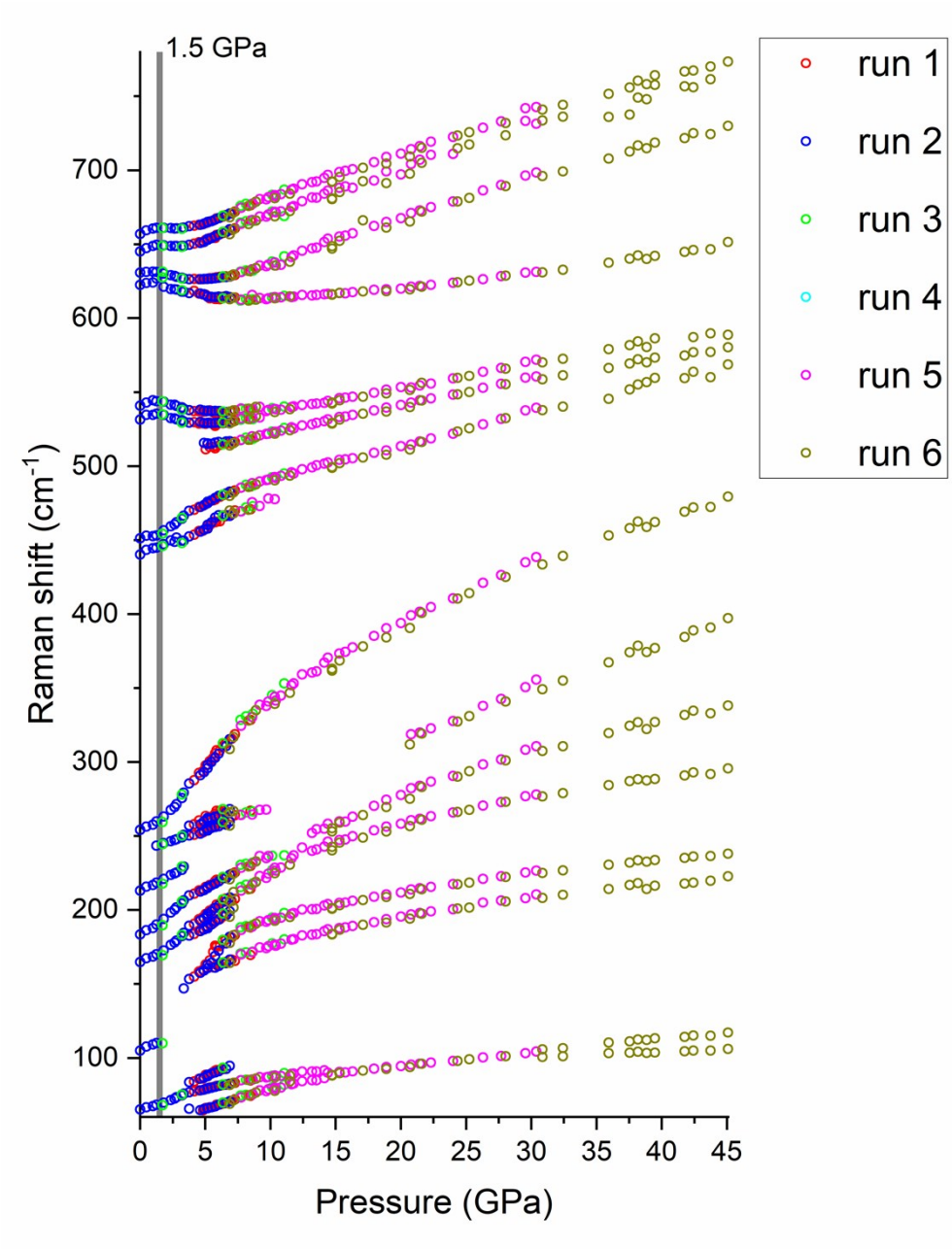

Fig. S 6 Pressure dependence of the frequencies of the Raman bands of solid AuF_3 measured upon compression (different colors mark different runs).

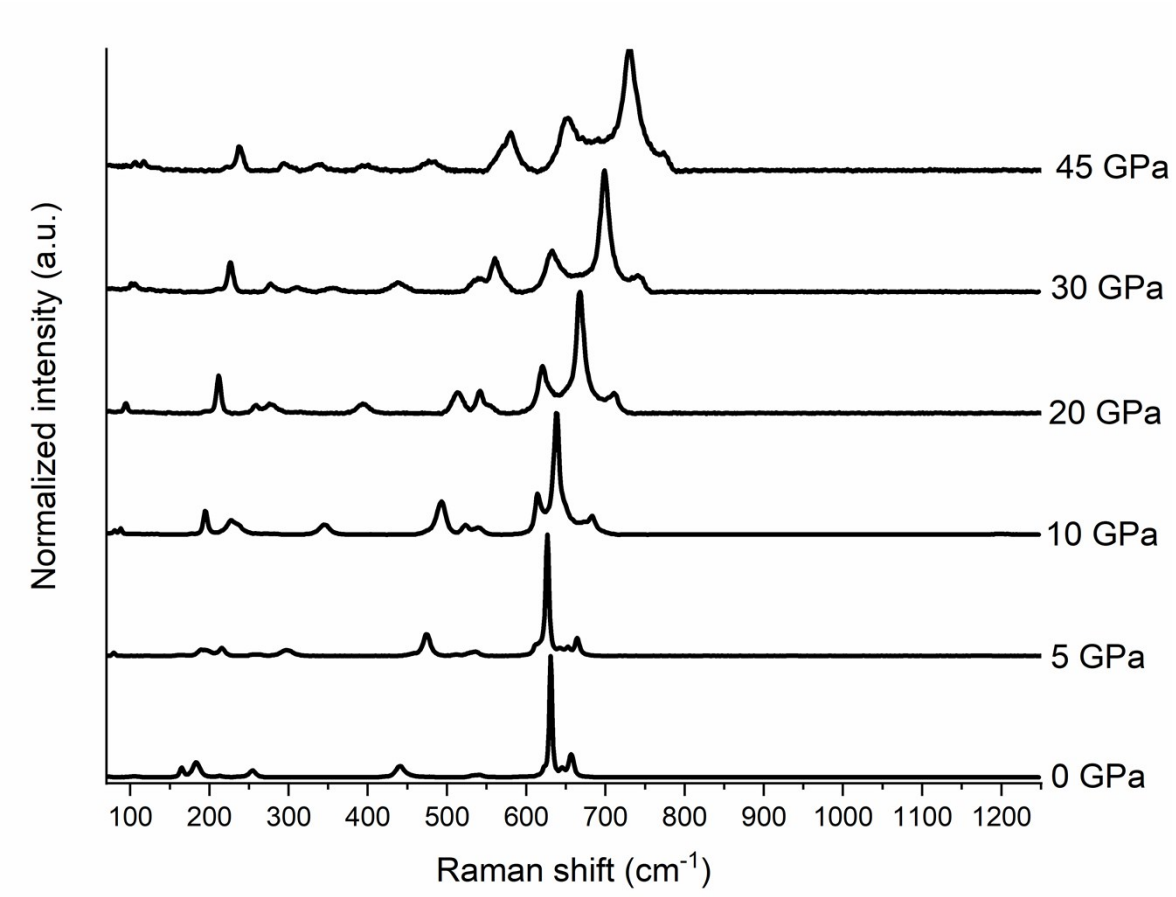

Fig. S 7 Comparison of the Raman spectra of compressed AuF_3 at selected pressures (spectra are offset for clarity).

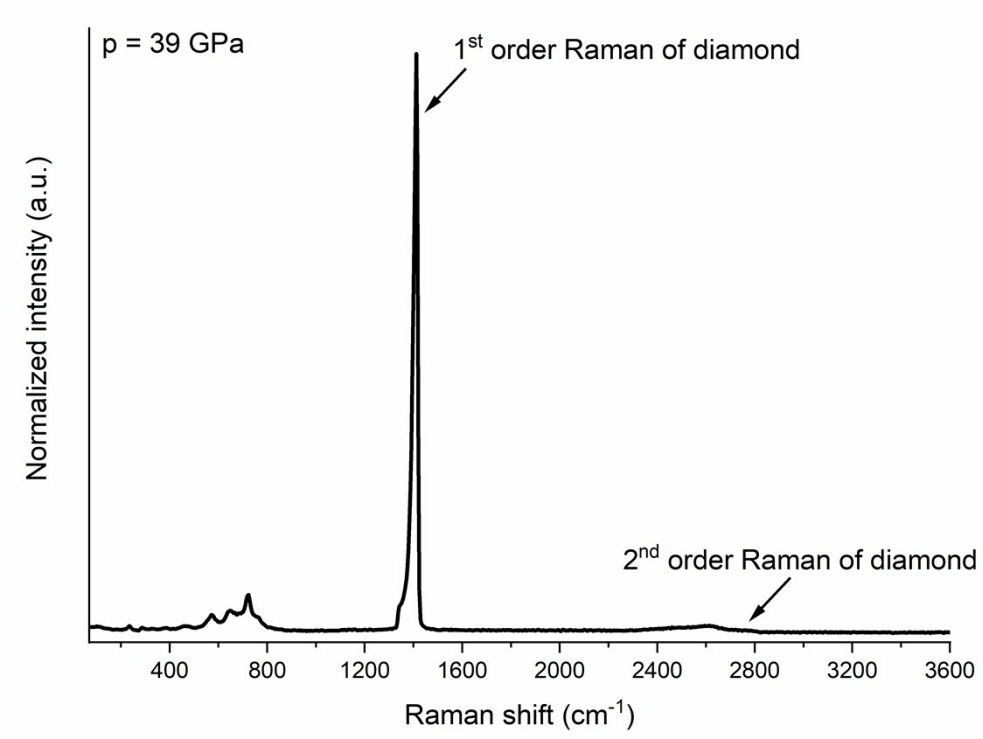

Fig. S 8 Extended range Raman spectrum of AuF_3 compressed confined in a DAC at 39 GPa.

Crystal structure of the novel high-pressure polymorphs of AuF_3

Structures optimized with SCAN and given below in VASP format.

P61 10 GPa

```
  1.00000000000000
    4.3748027567666048    0.0000019211749695    0.0000000000000000
   -2.1874030421696307    3.7886893634311019    0.0000000000000000
    0.0000000000000000    0.0000000000000000   16.8583856127128193
  Au   F
    6    18
Direct
 0.3738400234095351  0.3746267678221855  0.2563806795449395
 0.6253732041778122  0.9992132735873582  0.5897140605449422
 0.0007867874126433  0.6261599885904587  0.9230473555449450
 0.6261599525904629  0.6253731851778142  0.7563807085449383
 0.3746267598221849  0.0007867624126447  0.0897140605449422
 0.9992132195873609  0.3738400264095390  0.4230473845449438
 0.9183090076980349  0.7538152070911295  0.0324423391489788
 0.2461847939088671  0.1644937776069071  0.3657756801489782
 0.8355062733930936  0.0816910303019611  0.6991090041489798
 0.0816910333019649  0.2461847919088669  0.5324423571489802
 0.7538151990911288  0.8355062373930977  0.8657755961489784
 0.1644937616069058  0.9183089846980366  0.1991090041489798
 0.5795384982248564  0.0754251411965683  0.9880205002302134
 0.9245749418034279  0.5041133720282787  0.3213538802302125
 0.4958866259717212  0.4204615097751443  0.6546872042302141
 0.4204615017751436  0.9245749138034256  0.4880205562302109
 0.0754251471965688  0.4958866429717190  0.8213537952302090
 0.5041133970282843  0.5795385362248524  0.1546871902302129
 0.5873155901351055  0.8312520331142821  0.3034564560758710
 0.1687480168857221  0.7560635850208328  0.6367897800758655
 0.2439364379791726  0.4126844438648973  0.9701231880758669
 0.4126844248648922  0.1687479978857240  0.8034564270758651
 0.8312520181142773  0.2439364299791649  0.1367897800758655
 0.7560635720208353  0.5873156031351030  0.4701231040758671
```

C2_c_a (pr) 10 GPa

```
  1.00000000000000
    3.9035752866891102   -0.1189848993802109   -0.1431777998491730
   -0.6463259945999539    4.9105455350708587    0.0167703409590615
   -0.6518440924924354   -1.0240517832483966    4.8018326821234263
  Au   F
    2    6
Direct
 0.0590415299367161  0.8574544021449929  0.7656881333340257
 0.5589981354357004  0.3574183597412787  0.2657274150614742
 0.1477513107966659  0.1343211949633632  0.3313714930518468
 0.6477844523901057  0.9231207036413080  0.5425929337264603
 0.4702632668318504  0.7917818999196079  0.9887875195795321
 0.8089754098535858  0.4623667724644897  0.6608608831946006
 0.9702739609864771  0.5805041857644925  0.2001097438223262
 0.3090223137688882  0.2525720013604511  0.8706040982297689
```

C 2_c_b 30 GPa

```
  1.00000000000000
    6.4691300314068805    0.0000000000000000    0.0234967178343975
    0.0000000000000000    4.2616545207618222    0.0000000000000000
   -3.3975034015437315    0.0000000000000000   11.3354807883680113
```

Au F
8 24
Direct
0.9826028587195623 0.4999012084448681 0.4701376631334263
0.9826028587195623 0.5000987915551319 0.9701376331334236
0.4826028587195624 0.9999012084448681 0.4701376631334263
0.4826028587195624 0.0000987915551319 0.9701376331334236
0.9825117346564328 0.1265272024165468 0.7201066694421031
0.9825117346564328 0.8734728115834544 0.2201066694421031
0.4825117046564304 0.6265271884165456 0.7201066694421031
0.4825117046564304 0.3734728115834543 0.2201066694421031
0.1558605302952651 0.3778928610278049 0.3720176406896429
0.1558605302952651 0.6221071089721998 0.8720176406896428
0.6558605302952650 0.8778928910278002 0.3720176406896429
0.6558605302952650 0.1221071389721951 0.8720176406896428
0.0206514844785179 0.1107108543295730 0.8902659252085585
0.0206514844785179 0.8892891456704269 0.3902659252085585
0.5206514604785158 0.6107108543295731 0.8902659252085585
0.5206514604785158 0.3892891456704270 0.3902659252085585
0.9444800291409980 0.1104873422375776 0.5499710422769999
0.9444800291409980 0.8895126727624272 0.0499710422769999
0.4444800291409980 0.6104873272375728 0.5499710422769999
0.4444800291409980 0.3895126727624271 0.0499710422769999
0.7879052744679648 0.3692862034649759 0.2669621208724425
0.7879052744679648 0.6307138255350229 0.7669621208724425
0.2879052744679648 0.8692861744649771 0.2669621208724425
0.2879052744679648 0.1307137965350240 0.7669621208724425
0.3093233611102870 0.1218855177450941 0.5682679744665410
0.3093233611102870 0.8781144892549030 0.0682679744665409
0.8093233611102869 0.6218855107450970 0.5682679744665410
0.8093233611102869 0.3781144892549030 0.0682679744665409
0.6771447021309762 0.1307000862975800 0.6733109659102802
0.6771447021309762 0.8692998907024215 0.1733109659102803
0.1771447021309762 0.6307001092975785 0.6733109659102802
0.1771447021309762 0.3692999207024241 0.1733109659102803

References

1 M. Wojdyr, *J. Appl. Crystallogr.*, 2010, **43**, 1126–1128.

2 A. Dewaele, M. Torrent, P. Loubeyre and M. Mezouar, *Phys. Rev. B*, 2008, **78**, 104102.

3 Y. Akahama and H. Kawamura, *J. Appl. Phys.*, 2006, **100**, 043516.

4 J. Sun, A. Ruzsinszky and J. P. Perdew, *Phys. Rev. Lett.*, 2015, **115**, 036402.

5 B. Žemva, K. Lutar, A. Jesih, W. J. Casteel, A. P. Wilkinson, D. E. Cox, R. B. Von Dreele, H. Borrmann and N. Bartlett, *J. Am. Chem. Soc.*, 1991, **113**, 4192–4198.

6 P. E. Blöchl, *Phys. Rev. B*, 1994, **50**, 17953–17979.

7 G. Kresse and J. Furthmüller, *Phys. Rev. B*, 1996, **54**, 11169–11186.

8 G. Kresse and D. Joubert, *Phys. Rev. B*, 1999, **59**, 1758–1775.

9 P. Avery, C. Toher, S. Curtarolo and E. Zurek, *Comput. Phys. Commun.*, 2019, **237**, 274–275.

10 J. P. Perdew, K. Burke and M. Ernzerhof, *Phys. Rev. Lett.*, 1996, **77**, 3865–3868.

11 K. Refson, P. R. Tulip and S. J. Clark, *Phys. Rev. B*, 2006, **73**, 155114.

12 S. J. Clark, M. D. Segall, C. J. Pickard, P. J. Hasnip, M. I. J. Probert, K. Refson and M. C. Payne, *Zeitschrift für Krist. - Cryst. Mater.*, 2005, **220**, 567–570.

13 E. E. Zvereva, A. R. Shagidullin and S. A. Katsyuba, *J. Phys. Chem. A*, 2011, **115**, 63–69.

14 A. V. Krukau, O. A. Vydrov, A. F. Izmaylov and G. E. Scuseria, *J. Chem. Phys.*, 2006, **125**, 224106.

15 K. Momma and F. Izumi, *J. Appl. Crystallogr.*, 2011, **44**, 1272–1276.

16 H. T. Stokes and D. M. Hatch, *J. Appl. Crystallogr.*, 2005, **38**, 237–238.

17 T. Björkman, *Comput. Phys. Commun.*, 2011, **182**, 1183–1186.

18 E. Kroumova, M. I. Aroyo, J. M. Perez-Mato, A. Kirov, C. Capillas, S. Ivantchev and H. Wondratschek, *Phase Transitions*, 2003, **76**, 155–170.

19 M. A. Ellwanger, S. Steinhauer, P. Golz, H. Beckers, A. Wiesner, B. Braun-Cula, T. Braun and S. Riedel, *Chem. - A Eur. J.*, 2017, **23**, 13501–13509.